JOURNAL OF MATERIALS SCIENCE 20 (1985) 674–681

Phase-transition boundaries in 1,6-di(9-carbazolyl)-2,4-hexadiyne

D. BLOOR, I. F. CHALMERS, R. J. KENNEDY*
Department of Physics, Queen Mary College, Mile End Road, London, E1 4NS, UK
M. MOTEVALLI
Department of Chemistry, Queen Mary College, Mile End Road, London, E1 4NS, UK

1,6-di (9-carbazolyl)-2,4-hexadiyne has a first-order phase transition at 142 K at one atmosphere pressure. The boundaries between the high and low-temperature phase regions in single crystals were observed by optical microscopy and their dynamics recorded using video techniques. Crystal-lattice parameters measured close to the phase transition show that the commonest phase boundaries occur on crystallographic planes across which the lattice mismatch in the two structures is a minimum. Complex phase-boundary structures are observed in regions of high strain in the crystals. Repeated cycling through the transition leads ultimately to the destruction of the crystals.

1. Introduction

Di-substituted di-acetylenes have been extensively studied because of their ability to react in the solid state to form macroscopic polymer crystals, as shown schematically in Fig. 1. [1–6]. The physical properties of the polymer crystals are similar, being primarily determined by the conjugated polymer chains. The side groups play a secondary role though they can have a significant influence on certain properties, e.g. the optical absorption spectra [7] and the mechanical properties [8]. In contrast the properties of the monomer crystals are strongly dependent on the end groups, R and R′ of Fig. 1. The interactions between the end groups largely determine whether a solid-state reaction is possible and the quality of any polymer produced [5]. This follows since the crystal structures of diacelytene monomers are primarily determined by the end groups.

Many disubstituted diacetylenes are flexible molecules which can adopt different conformations, in consequence they are often polymorphic and can undergo solid-state phase transformations from one form to another [9, 10]. In many reactive diacetylenes the phase transitions disappear on polymerization since the polymer chains prevent the necessary molecular rearrangement from occurring. A typical example is 1,6-di(carbazolyl)-2,4-hexadiyne (DCH) which has the chemical structure shown in Fig. 2.

DCH was first studied because of its ability to form high quality, polymer crystals by either X-ray or γ-ray polymerization. [11–13]. The mechanical, optical and electronic properties of this polymer have been studied subsequently [14–18] together with the polymerization of pure and co-crystallized samples [19–20]. During these studies it was found that the monomer undergoes a first-order phase transition at 142 K with an unusually large change in crystal density [19]. The large dimensional changes associated with this phase transitions result in:

(i) a distinct colour change for crystals containing a trace of polymer [21] and
(ii) an extreme sensitivity of the transition temperature to hydrostatic pressure [22].

The former effect occurs because at very low polymer concentrations the polymer chains are forced to conform with the monomer lattice. For DCH this means that the polymer is compressed by approximately 8% at room temperature and by

*Present address: Department of Metallurgy, University of Strathclyde, Glasgow, Scotland, UK.

0022–2461/85 $03.00 + .12

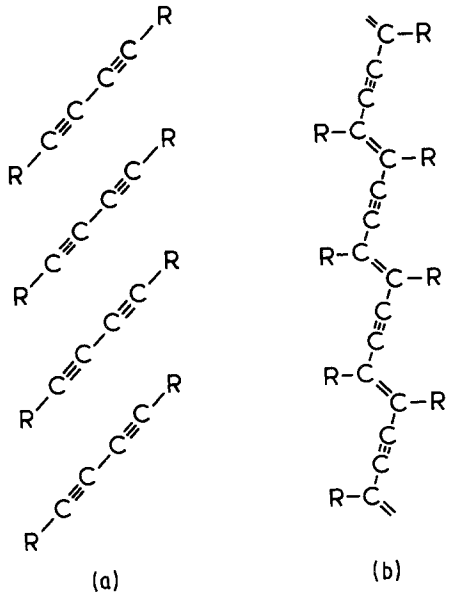

Figure 1 Diacetylene monomer molecules arranged in a reactive stack (a) leading to the formation of extended-chain polymer (b), schematic diagram.

approximately 14% at 120 K. This results in a shift of 3540 cm^{-1} in the polymer absorption at the phase transition with a visual change from blue to red on cooling through the transition [21]. This colour change facilitated the observation of the phase transition under hydrostatic pressure. The rate of change of transition temperature at 142 K was found to be 0.63 ± 0.08 K MPa^{-1} decreasing to 0.48 ± 0.05 K MPa^{-1} at 300 K.

During these studies the occurrence of distinct phase-transition boundaries, domain structures and deformation of the crystals were noted [21]. The nucleation of the second phase, both on heating and cooling, occurred in the vicinity of crystal defects and usually after a few cycles through the transition enough strain was developed to shatter the crystals. We have subsequently investigated these effects by optical microscopy and have recorded the dynamics of the phase transition interfaces using video techniques. In addition new X-ray determinations of the lattice parameters of DCH were made in order to assist in the interpretation of the microscopic observations. A brief account of this work has appeared elsewhere [23]. A more detailed report is present below.

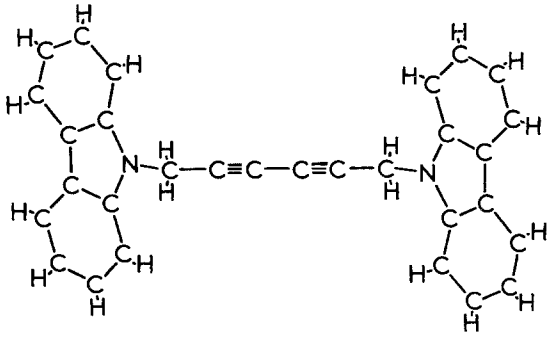

Figure 2 Molecular structure of 1,6-di(carbazolyl)-2,4-hexadiyne (DCH) after the crystal structure of [20].

2. Experimental method

DCH was prepared by the coupling of 3-(9-carbazolyl)-1-propyne as described by Yee [12]. The precursor was prepared using butyl lithium as reagent since this was found to give a product which could be purified more readily than that prepared by the method of Yee [12] and Yee and Chance [14]. Elemental analysis of the DCH gave C: 87.82%, H: 4.79% and N: 6.75% compared with calculated values of C: 88.21%, H: 4.93% and N: 6.86% for the formula unit of Fig. 2. Fine needle-like single crystals suitable for microscope observations were grown, by slow evaporation, from toluene solution.

Unit-cell parameters were determined using a four-circle, automatic diffractomer, Enraf-Nonius CAD4. The crystals were mounted in Lindemann tubes and cooled in a nitrogen gas stream the temperature of which could be controlled from room temperature to about 100 K with an accuracy of ± 1 K. As noted by other workers polymerization in the X-ray beam is slow even at room temperature [11, 14, 19]; to eliminate errors due to any polymerization, separate crystals were used for the room and low-temperature determinations. The positions of up to twenty five high-angle, intense reflections were determined and automatically centred. The lattice parameters were obtained by least-squares fitting of the setting angles of these reflections. Cu$K\alpha$ radiation was used for these determinations.

A Zeiss Universal photomicroscope was used for visual observations. The crystals were mounted on a thin glass side which was cooled from underneath by a stream of argon from an EMI Joule-Thompson refrigerator. The refrigerator is small enough to be mounted directly on the microscope stage as shown schematically in Fig. 3. The sample temperature can be controlled to within 0.1 K by adjusting the gas temperature and flow rate of the high pressure inlet gas. The former is varied by partial immersion of a cooling coil in liquid

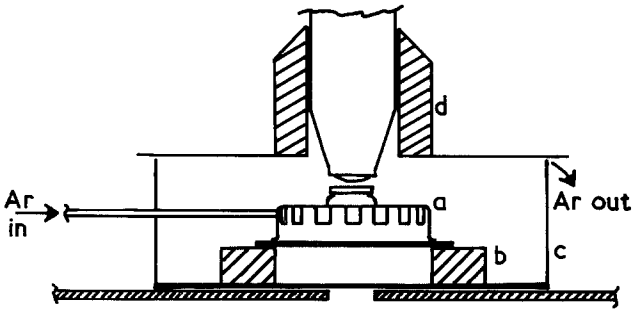

Figure 3 Experimental arrangement used for low-temperature microscopy; a – Joule–Thompson cooler; b – insulating supports, c and d – polystyrene enclosure with loose fitting lid. Argon gas vents from the cooler filling the enclosure with dry gas.

nitrogen and the latter by a needle valve in the gas feed-line. The gas exhaust from the cooler is contained in a plastic shroud fitted to the microscope objective. This blanket of cold, dry gas prevents condensation from occurring on the crystals and slide.

The dynamics of the phase-transition boundaries were recorded by mounting a TV camera above the microscope vertical-beam exit normally used for either spectroscopy or photometry. The camera output was viewed on a monitor and recorded on a video recorder.

Photographic records were obtained either directly utilizing the intergral 35 mm microscope camera or indirectly by photographing single frames of the video recording from the monitor.

3. Results and discussion

The DCH monomer crystals were obtained in the form of thin, flat needles elongated along the *b* axis with well defined {1 0 0}, {1 0 2} and {1 0 2} facets, as reported by Enkelmann *et al.* [19]. The most prominent facets are the {1 0 0} facets so that the crystals are normally viewed in the microscope perpendicular to the *bc* lattice plane. Typical examples of phase-transition boundaries observed in such crystals are shown in Figs. 4, 5 and 6.

During the first few cycles through the transition temperature single, well defined boundaries can be observed in the best crystals, as shown in Fig. 4. These features are readily identified as phase-transition boundaries by the abrupt colour change which occurs at the boundary. Phase-transition boundaries have been observed orientated along the [0 3 1], [0 3 $\bar{1}$], [0 4 1] and [0 4 $\bar{1}$] directions, i.e. coincident with the {0 1 3}, {0 $\bar{1}$ 3}, {0 1 4} and {0 $\bar{1}$ 4} lattice planes. The latter boundaries are much less common than the former. The boundaries in Fig. 4 lie along either [0 3 1] or [0 3 $\bar{1}$], in the small crystals used in these experiments it is not possible to distinguish between these two directions. The phase-transition boundaries were identified by using the lattice parameters listed in Table I. This information can also be used to determine the deformation at the phase boundaires and to explain the occurrence of only two different boundaries.

As can be seen in Table I our room-temperature data is in excellent agreement with that of Enkelmann *et al.* [19, 20]. Our data taken at 155 K is less accurate than the room-temperature data indicating some build up of strain in the sample. Below the transition temperature strain and deformation in our crystals were too great to

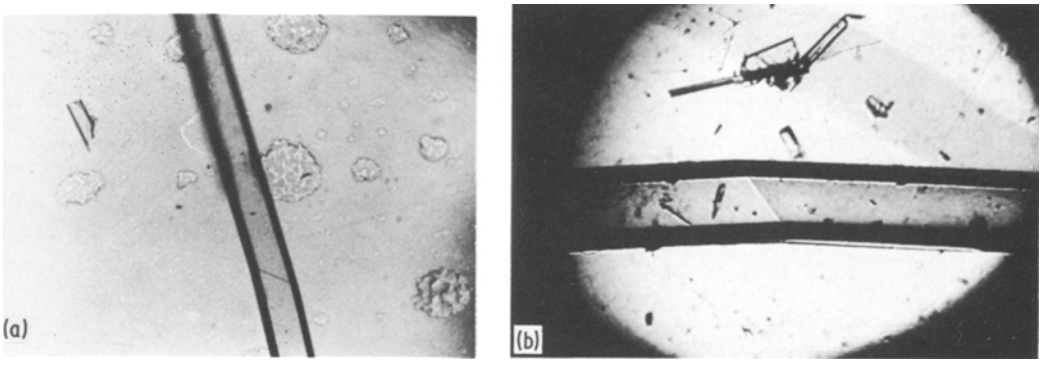

Figure 4 Single crystals of DCH showing single, sharp, phase-transition boundaries, (a) direct micrograph and (b) photograph from video monitor. The deviation of the crystal produced by the boundary is clearly visible.

TABLE I Lattice parameters of DCH monomer as a function of temperature. The standard deviation in the least significant figure is shown in brackets

	Temperature (K)			
	300 [19, 20]	300	155	120 [19, 20]
a (×10 nm)	13.60(4)	13.629(1)	13.529(8)	13.28(1)
b (×10 nm)	4.55(3)	4.5394(5)	4.527(2)	4.20(5)
c (×10 nm)	17.60(4)	17.632(2)	17.54(1)	18.44(1)
β (°)	94.0(5)	93.379(6)	93.110(5)	92.0(5)
D_c (g cm^{-3})	1.25	1.246	1.265	1.31
Z	4	4	4	4
Space group	$P2_1/c$	$P2_1/c$	$P2_1/c$	$P2_1/c$

enable us to obtain structural data, therefore, we use the 120 K data of Enkelmann *et al.* [19, 20]. The parameters measured at 155 K show that the crystal density increases due to thermal contraction and that at the phase transition the changes in a and b-axes are smaller and that in the c-axis is larger than indicated by the room-temperature lattice parameters.

The calculated and observed angles between the phase-transition boundaries and the crystal b-axis are listed in Table II. For both crystallographic planes there is a deviation of the b-axis about 3.5°.

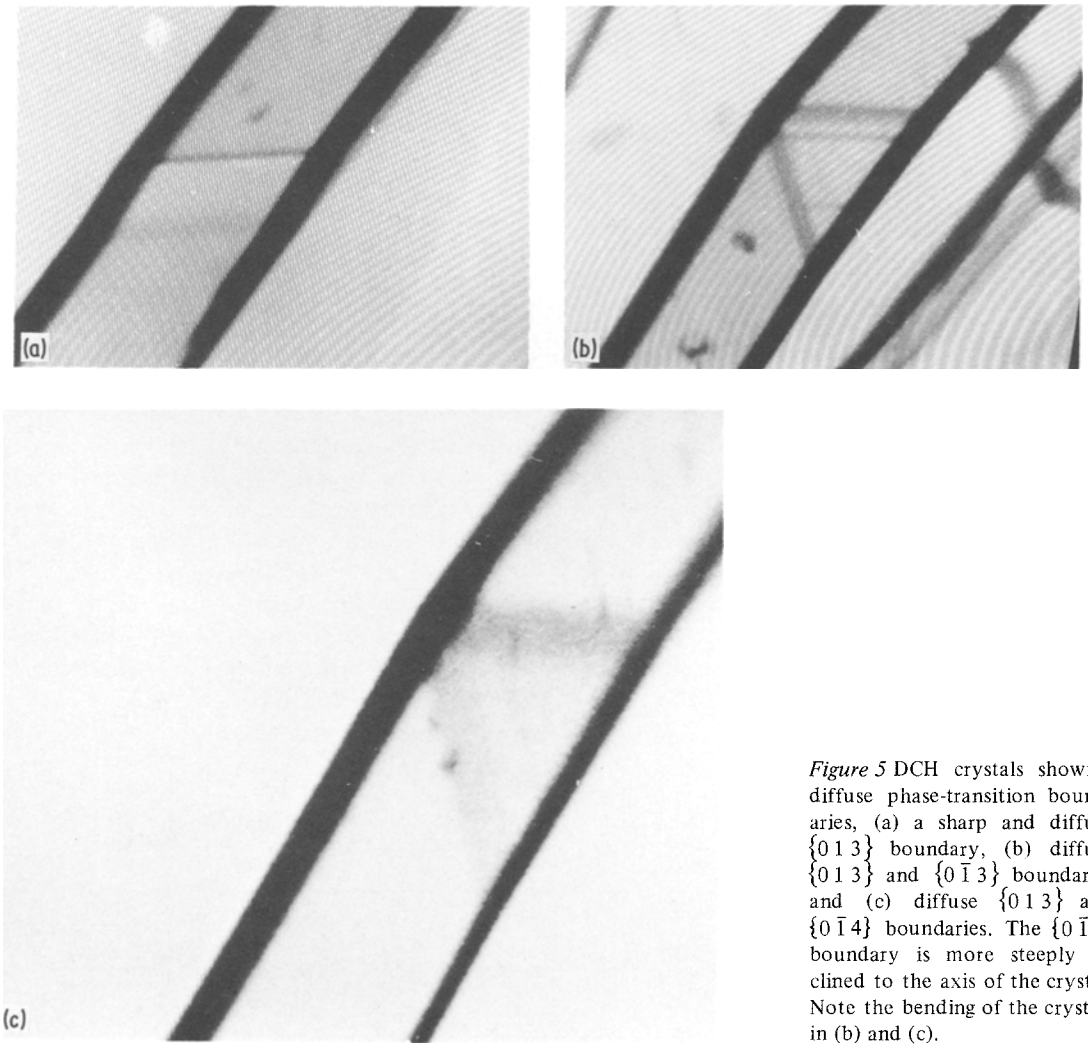

Figure 5 DCH crystals showing diffuse phase-transition boundaries, (a) a sharp and diffuse $\{0\,1\,3\}$ boundary, (b) diffuse $\{0\,1\,3\}$ and $\{0\,\bar{1}\,3\}$ boundaries and (c) diffuse $\{0\,1\,3\}$ and $\{0\,\bar{1}\,4\}$ boundaries. The $\{0\,\bar{1}\,4\}$ boundary is more steeply inclined to the axis of the crystal. Note the bending of the crystals in (b) and (c).

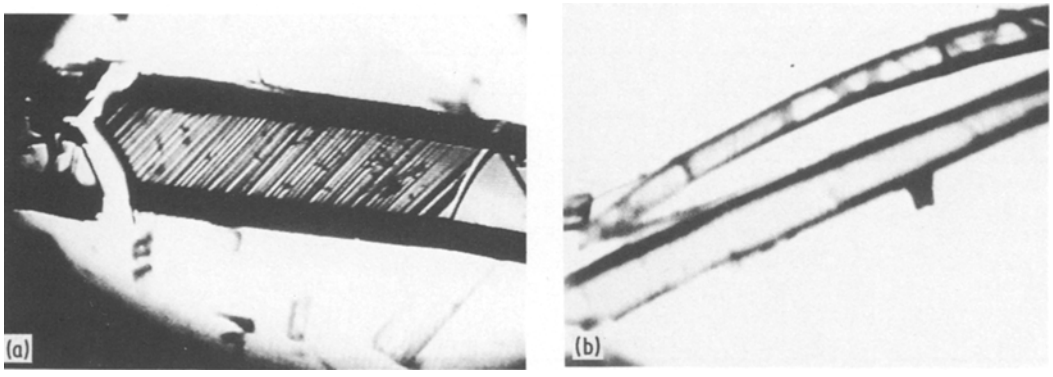

Figure 6 DCH crystals showing the development of extended, multiple, phase-transition boundaries, (a) multiple $\{0\,1\,3\}$ boundaries and (b) multiple $\{0\,1\,3\}$ and $\{0\,\bar{1}\,3\}$ boundaries producing macroscopic bending in the upper crystal.

This deviation can be clearly seen in Figs. 4 and 5. Since in both phases the crystal lattice is close to an orthorhombic structure, β is 93° in the high-temperature phase and 92° in the low, the deviation at the boundary is principally a rotation about the *a*-axis. There is, however, a smaller rotation about the *c*-axis, this can be seen in Fig. 4a by the loss of focus indicating lack of planarity of the sample. Assuming that the normals to the lattice planes forming the phase-transition boundaries are coincident then the deviations at the boundaries are as given in Table III. The relationship of the normals for the $\{0\,1\,3\}$ plane in the high and low-temperature phases is shown in Fig. 7a.

The reason for the predominance of $\{0\,1\,3\}$ phase boundaries, the results shown in Figs. 4, 5 and 8 are typical, is that these boundaries have the lowest strain energy, i.e. the smallest dimensional changes between high and low-temperature phases. This is illustrated in Table IV which lists the areas of the $\{0\,1\,n\}$ planes and the lengths in the $[0\,n\,1]$ directions within a single unit cell and the fractional changes in these quantities. The $\{0\,1\,3\}$ plane has changes in area of -0.4% and length of $+0.7\%$ which are both minima for $\{0\,1\,n\}$ planes. The changes for $\{0\,1\,2\}$ and $\{0\,1\,4\}$ planes are similar, however, though $\{0\,1\,4\}$ planes are occasionally observed, see Fig. 5, no $\{0\,1\,2\}$ planes have yet been detected.

In addition to the sharp boundaries as shown in Fig. 4, diffuse boundaries are also observed, Fig. 5. Both sharp and diffuse boundaries occur as multiple-boundary domain structures in samples that have been cycled through the phase transition several times. It is possible that the diffuse boundaries may be sharp boundaries viewed away from edge-on. This, however, seems unlikely since the deviation of the crystals are the same at sharp and diffuse phase-transition boundaries, cf. the boundaries in Fig. 5a and the crystal deformation in Figs. 4 and 5b and c. Thus, it seems probable that the diffuse boundaries consist of numerous sub-boundaries, with alternating narrow layers of high and low-temperature phase which are too narrow to be resolved. Such structures usually appear after several cycles through the phase transition together with other evidence of a build up of strain in the crystals, e.g. the cleavage of the crystal in Fig. 6a. The local strain at the phase-transition boundary must be high, cf. Table I, and leads eventually to cleavage of the crystals as discussed below. Nucleation of the new phase is usually observed at the site of diffuse or multiple

TABLE II Angular separation of the crystal *b*-axis and the $\{0\,1\,n\}$ lattice planes in the *bc*-plane, all values in degrees. Calculated values were obtained from crystallographic data recorded at 155 and 120 K. Observed values were measured at 142 K

Phase	$n = 2$		$n = 3$		$n = 4$	
	calc	obs	calc	obs	calc	obs
High temperature	62.7	–	52.2	51 ± 1	44.1	44 ± 2
Low temperature	65.5	–	55.7	55 ± 1	47.7	46.5 ± 2

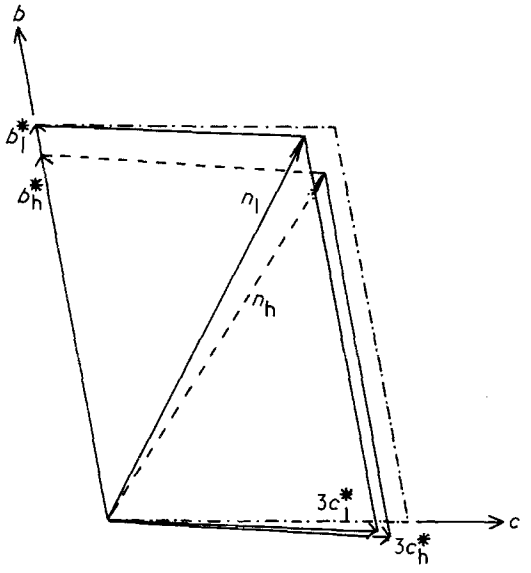

Figure 7 Orientations of the normals to the $\{0\,1\,3\}$ plane in the high temperature (n_h) and low temperature (n_l) phases relative to the crystal *bc*-plane (shown by chain lines).

boundaries, this is further evidence for local strain since the transition temperature is very sensitive to lattice deformation, e.g. with hydrostatic pressure [22]. As noted earlier the transition temperature is shifted at $0.63\,\mathrm{K\,MPa^{-1}}$ at 142 K, thus, a local strain equivalent to the deformation produced by a 1 atmosphere hydrostatic pressure can shift the transition temperature by about 0.1 K. Whereas hydrostatic pressure can produce only an increase in transition temperature, strain may result in both local increases and decreases in transition temperature. Hence, nucleation of the phase transition is likely to occur in strained crystal regions on both cooling and heating.

TABLE III Angular deviations of the *b*-axis across phase-transition boundaries on the $\{0\,1\,n\}$ lattice planes, the angles are measured about the a^*- and *c*-axes. All values in degrees

	$n = 3$	$n = 4$	observed $\{0\,1\,3\}$
$\phi\,(a^*)$	3.55	3.38	3.5
$\phi\,(c)$	1.27	0.95	–

Clearer evidence of the build up of internal strain as shown in Figs. 6, 8, 9. In Fig. 6a an extended region of thin lamellae of the high and low-temperature phases occur in a strained region, which has been fractured at both ends. Nucleation of the phase transition and the fracture of this crystal are shown in Fig. 8. Note the much higher density of boundaries observed after further thermal cycles in Fig. 6a. In Fig. 6b the upper part of the crystal has cleaved off from the bulk. The occurrence of sets of symmetry-related $\{0\,1\,3\}$ boundaries leads to a distinct bending of this part of the crystal. The mean transition temperature is obviously somewhat different in the two portions of the crystals since the upper part contains many phase boundaries while the lower part has none. In

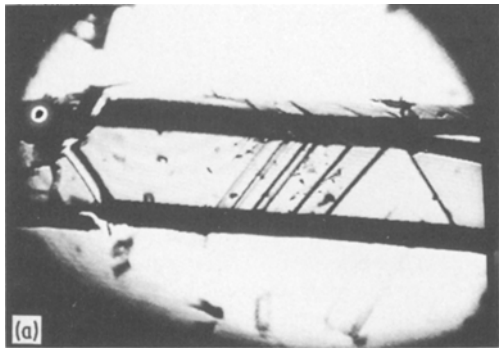

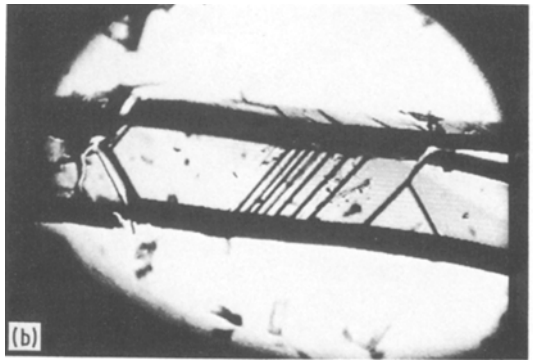

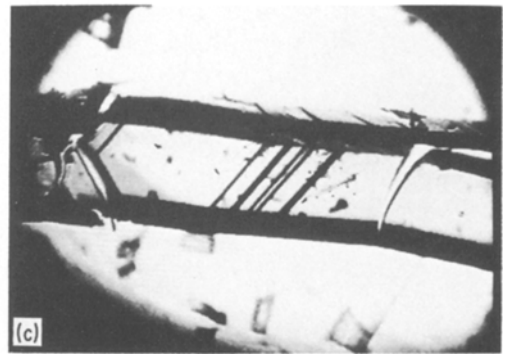

Figure 8 Concoidal fracture produced by annihilation of a $\{0\,1\,3\}$, $\{0\,\bar{1}\,3\}$ pair of phase-transition boundaries. (a) Boundaries (at right) prior to annihilation, (b) boundaries colliding and initial fracture of crystal and (c) fractured crystal. Note formation and annihilation of $\{0\,1\,3\}$ boundaries in the central portion of the crystal without failure of the crystal.

TABLE IV Dimensions and areas of phase-transition boundaries in DCH deduced from crystal-structure data. l is the separation of (0, 0, 0) and (0, 1, $1/n$) in units × 10 nm and A is the area within one unit cell of the $\{0\,1\,n\}$ plane in units of × 100 nm^2

Temperature (K)	l					A				
	$n=1$	$n=2$	$n=3$	$n=4$	$n=5$	$n=1$	$n=2$	$n=3$	$n=4$	$n=5$
155	18.11	9.87	7.39	6.30	5.73	244.8	133.4	99.95	85.21	77.44
120	18.91	10.13	7.44	6.24	5.59	252.9	135.5	99.58	83.12	74.64
Δ (%)	+4.4	2.7	+0.7	−1.05	−2.4	+3.3	+1.6	−0.4	−2.5	−3.6

extreme cases crystals have been observed to bend through almost 360° due to the presence of such complex phase boundary structures. After the appearance of these domain structures the crystals are usually shattered into small fragments by a few further cycles through the transition, providing more evidence of the rapid build up of strain in the crystals.

Two distinct mechanisms of fracture have been observed. Cleavage parallel to the crystal b-axis can occur by rapid passage of a single phase-transition boundary. In one sequence recorded on video tape shown in Figs 9, such a cleavage crack was observed to follow the phase boundary during cooling. The cleavage did not extend along the whole length of the crystal and was partially healed by a boundary propagating in the opposite direction during heating. Further cycling caused growth of the crack and eventually the new phase nucleated at the crack tip. Several other examples of closure of cleavage cracks have been observed. Cleavage in the ac-plane, which can be seen in Fig. 9c, and concoidal fractures are produced by the annihilation of a pair of $\{0\,1\,3\}$ and $\{0\,\bar{1}\,3\}$ phase boundaries, as shown in Fig. 8. Consideration of the molecular packing [19, 20] shows that ac-cleavage will be less favourable than cleavage parallel to the b-axis, hence concoidal fracture is likely to compete with ac-cleavage. The higher strain fields necessary for these processes are generated only when two boundaries with different orientations impinge on one another. This is a relatively rare event for good crystals during the initial cycles through the transition but becomes more likely as the strain, and complex boundary structures develop after several cycles through the transition. Thus, repeated thermal cycling eventually leads to destruction of the crystals.

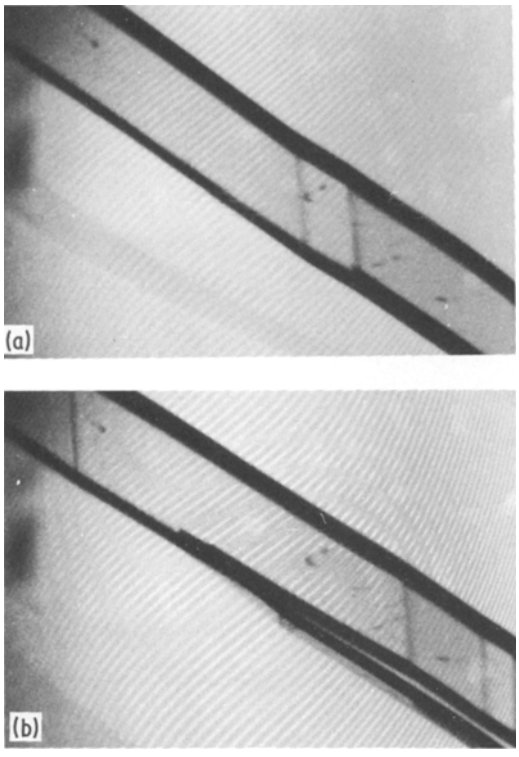

Figure 9 Propagation of a cleavage crack along a DCH crystal. (a) Nucleation of phase transition at the crack tip, (b) crack propagation following movement of transition boundaries and (c) separation of cleaved crystal fragment by subsequent cleavage on the ac-plane.

4. Conclusions

The behaviour of crystals of 1,6-di(9-carbazolyl)-2,4-hexadiyne at the first-order phase-transition at

142 K has been studied in detail. Crystal lattice parameters measured close to the transition have been used to explain the appearance of particular phase boundaries, the deformation of crystals containing phase boundaries and the break up of crystals after several cycles through the phase transition.

Acknowledgements

This work was supported by grants from the Science and Engineering Research Council.

References

1. G. WEGNER, "Molecular Metals", edited by W. E. Hadfield (Plenum Press, New York, 1979), p. 209.
2. *Idem, Faraday Disc.* **68** (1980) 494.
3. R. H. BAUGHMAN and R. R. CHANCE, *Ann. New York Acad. Sci.* **313** (1978) 705.
4. D. BLOOR, "Recent Advances in the Quantum Theory of Polymers", Springer Lecture Notes in Physics Vol. 113, edited by J. M. Andre, J. L. Bredas, J. Delhalle, J. Ladik, G. Leroy and K. Moser (Springer, 1980) p. 14.
5. *Idem*, "Developments in Crystalline Polymers", Edited by D. C. Bassett (Applied Science Publ., London, 1982) p. 151.
6. H. SIXL, *Adv. Polm. Sci.* **63** (1984) 49.
7. D. BLOOR, *Amer. Chem. Soc. Symp. Ser.* **162** (1981) 81.
8. C. GALIOTIS, R. J. YOUNG, D. J. ANDO and D. BLOOR, *Makromol. Chem.* **184** (1983) 1083.
9. G. WEGNER, *Z. Naturforsch* **24b** (1969) 824.
10. D. J. ANDO, D. BLOOR, C. L. HUBBLE and R. L. WILLIAMS, *Makromol. Chem.* **181** (1980) 453.
11. V. ENKELMANN, G. SCHLEIER, G. WEGNER, H. EICHELE and H. SCHWOERER, *Chem. Phys. Lett.* **52** (1977) 314.
12. K. C. YEE, US Patent US 412 5534 (1978).
13. P. A. APGAR and K. C. YEE, *Acta Crystallogr.* **B34** (1978) 957.
14. K. C. YEE and R. R. CHANCE, *J. Polym. Sci. Polym. Phys. Ed.* **16** (1978) 431.
15. C. GALIOTIS, Thesis, University of London, UK (1982).
16. R. J. HOOD, H. MULLER, C. J. ECKHARDT, R. R. CHANCE and K. C. YEE, *Chem. Phys. Lett.* **54** (1978) 295.
17. W. SPANNRING and H. BASSLER, *ibid.* **84** (1982) 54.
18. R. J. YOUNG, C. GALIOTIS, D. BLOOR and I. F. CHALMERS, *J. Polym. Sci. Polym. Phys. Ed.* **22** (1984) 1589.
19. V. ENKELMANN, R. J. LEYRER, G. SCHLEIER and G. WEGNER, *J. Mater. Sci.* **15** (1980) 168.
20. V. ENKELMANN, G. SCHLEIER and H. EICHELE, *ibid.* **17** (1982) 533.
21. R. J. KENNEDY, I. F. CHALMERS and D. BLOOR, *Makromol. Chem. Rapid Comm.* **1** (1980) 357.
22. R. J. LACEY, R. L. WILLIAMS, R. J. KENNEDY, D. BLOOR and D. N. BATCHELDER, *Chem. Phys. Lett.* **83** (1981) 65.
23. D. BLOOR, I. F. CHALMERS, R. J. KENNEDY and M. MOTEVALLI, *Mol. Cryst. Liq. Cryst.* **93** (1983) 215.

Received 21 March
and accepted 12 April 1984